Surface Review and Letters, Vol. 5, No. 5 (1998) 1087–1106


# DIRECT METHODS FOR SURFACES

L. D. MARKS, E. BENGU, C. COLLAZO-DAVILA, D. GROZEA, E. LANDREE,
C. LESLIE and W. SINKLER
*Department of Materials Science and Engineering, Northwestern University,*
*Evanston, IL 60208, USA*

Received 17 March 1998

This paper reviews recent progress in the application of Direct Methods to solve surface structures using surface X-ray or transmission electron diffraction data. The basic ideas of (crystallographic) Direct Methods are presented, as well as the additional problems posed by trying to apply them to surfaces and how they connect to the mathematical theory of projections. Surface crystallography notation is presented, which differs from the widely used LEED notation in that it emphasizes the surface symmetry. This is followed by a description of methods for structure completion and refinement, followed by applications to some experimental systems, both those where the structure was previously known (calibration tests) and a few where it was not, concluding with problems and limitations.

## 1. Introduction

To determine a surface structure, almost without exception the following strategy has been pursued to date: a set of experimental measurements is compared to models of the surface. The latter may be just approximate positions of the atoms accurate to perhaps 0.1 Å, or the positions may be varied to obtain the best fit. Using some criteria of the "goodness of fit," which model can best explain the experimental data is determined and described as best. While this is a powerful approach, it has one fundamental flaw: if the true structure does not belong to the set of models initially considered, then it will (almost without exception) never be found. With a simple system such as carbon monoxide on a nonreconstructed metal surface in a $1 \times 1$ or $2 \times 1$ cell, there are only a few possibilities. However, as the number of atoms in the cell increases, it rapidly becomes impossible to consider all the alternatives.

To overcome this problem, one has to be able to start from something rather close to the correct structure, then refine the atomic positions. Many techniques can do the latter step rather precisely if the initial positions are no more than 0.1–0.2 Å off. Patterson functions are one way of generating the initial guess since they give information about interatomic spacings, but can be difficult to use with complicated structures. An alternative is to use a real space imaging technique such as STM,[1–5] AFM[5] or HREM.[6–9] However, all have their problems. With STM and AFM not all atoms may be resolved and it can be difficult or impossible to tell the chemical nature of "features" in the images. As such, while they may constrain the symmetry of the structure, they may not give the required estimate of the atomic positions. HREM images are much easier to interpret, and do give atomic positions to the required level of accuracy. However, they suffer from substantial noise problems due to weak signals, although this will improve in the future with the use of brighter sources.

For bulk X-ray diffraction exactly the same issues were faced some years ago, and they have largely been solved by what are called Direct Methods.[10–12] Direct Methods can be broadly defined as the set of methods which provide an initial estimate of the atomic positions. As such they include Patterson-based techniques as well as (in a surface context) approaches such as Photoelectron Holography.[13–21] In a more crystallographic setting Direct Methods are a set of mathematical techniques for determining the phases of diffracted beams given only amplitude

Table I. List of surface structures solved by Direct Methods. * marks structures analyzed as calibration tests.

| Structure | Data | Reference |
|---|---|---|
| Si(111)-($\sqrt{3}\times\sqrt{3}$)R30°Au* | electron | 22 |
| Si(111)-(5 × 2)Au* | electron | 22 |
| Si(111)-(7 × 7)* | electron | 23 |
| Si(111)-(4 × 1)In | electron | 24 |
| Si(111)-(6 × 6)Au | X-ray | 28 |
| $TiO_2$(100)-(1 × 3) | X-ray | 29 |
| Si(111)-(3 × 1)Ag | electron | 25 |
| Si(111)-($\sqrt{3}\times\sqrt{3}$)R30°Ag* | electron | 30 |
| Ge(111)-(4 × 4)Ag | X-ray | 31 |
| MgO(111)-($\sqrt{3}\times\sqrt{3}$)R30° | electron | 32 |
| MgO(111)-(2 × 2) | electron | 32 |
| MgO(111)-($2\sqrt{3}\times 2\sqrt{3}$)R30° | electron | 32 |
| Ni(111)-($5\sqrt{3}\times 2$)S* | X-ray | – |
| Cu(111)-$\begin{vmatrix} 4 & 1 \\ -1 & 4 \end{vmatrix}$S* | X-ray | – |
| Cu(110)-p(4 × 1)Bi* | X-ray | – |

information, the square root of the measured intensities. In general they are much more powerful than Patterson techniques and at the time of writing have been used to solve three-dimensional structures containing more than 1000 independent atoms. Until very recently it was thought that these could not be used for surfaces, but we have lately been able to use them not just in two dimensions[22–25] but (very recently) for full three-dimensional solutions.[26]

In this review we will focus upon a general description of the method, primarily cases where the structure had already been determined by other techniques; cases where the structure was determined solely via direct methods will be included only if they are already in print. The structure of this review is as follows. The first section describes the basic ideas of (crystallographic) Direct Methods, as well as the additional problems posed by trying to apply them to surfaces. The next section describes a more general, and powerful, description using the method of Projection onto Sets.[27] After this we will describe briefly (for reference) surface crystallography notation in a conventional fashion, which differs from the widely used LEED notation for important reasons. This is followed by methods for structure completion and refinement, then applications to some experimental systems, both those where the structure was previously known (calibration tests) and others where it was not; Table I shows a list of cases where it has been applied to date with appropriate references.[22–25,28–32] We conclude with a description of (current) problems and limitations, which hopefully will be resolved in the future, with a short discussion at the end.

## 2. Basics

### 2.1. *What are Direct Methods?*

We have a set of $M$ (experimental) diffraction intensities, and by taking the square root have the moduli of the structure factors. The task we face is finding values of the $M$ phases to go with these moduli; when this is done all that is required is to take a Fourier transform to generate the real space potential (for transmission electron diffraction) or charge density (for X-ray diffraction), provided that we are dealing with kinematical data which is a good approximation in both cases. (Except for the structure factors there are few differences between the two; see also the discussion.) Even in the simplest case, such as a centrosymmetric structure (where the phase is either 180° or 360°), this sounds like an impossible task since the number of possible permutations is $2^M$. However, the phases cannot be totally random, which can be shown via many different routes, all of which lead to similar conclusions. We will give here a short description, based upon the idea that the scattering comes from atoms.

Consider a material with only one type of atom. The structure factor $F(\mathbf{k})$ as a function of the reciprocal lattice vector $\mathbf{k}$ can be written as

$$F(\mathbf{k}) = \sum_{\mathbf{r}_l} f(\mathbf{k})\, \exp(2\pi i \mathbf{k}\cdot\mathbf{r}_l)\,, \qquad (1)$$

where the sum is over the positions of the atoms $\mathbf{r}_1$ and $f(\mathbf{k})$ is the scattering from a single atom. (Throughout this paper we will use crystallographic notation with "$2\pi$" in Fourier transforms, not physics notation.) Dividing both sides by $Nf(\mathbf{k})$, where $N$ is the number of atoms, we generate the equation

$$U(\mathbf{k}) = F(\mathbf{k})/Nf(\mathbf{k}) = 1/N \sum_{\mathbf{r}_l} \exp(2\pi i \mathbf{k}\cdot\mathbf{r}_l)\,, \quad (2)$$

with $U(\mathbf{k})$ being called the unitary structure factor. [When there is more than one type of atom, $f(\mathbf{k})$ in

Eq. (2) should be replaced by the expectation value for random atomic coordinates $\langle f(\mathbf{k})^2\rangle^{1/2}$. There are also established methods in the literature for determining and correcting for Debye–Waller factors; we have yet to find a case where they work for surfaces.] Looking at the real space form of $U(\mathbf{k})$ (after a Fourier transform) $u(\mathbf{r})$,

$$u(\mathbf{r}) = (1/N) \sum_{\mathbf{r}_1} \delta(\mathbf{r} - \mathbf{r}_1)\,, \tag{3}$$

a set of delta functions at each of the atom sites. Since the square of a delta function is also a delta function,

$$u(\mathbf{r}) = N u(\mathbf{r})^2\,, \tag{4}$$

or, in reciprocal space,

$$U(\mathbf{k}) = N \sum_{\mathbf{h}} U(\mathbf{k} - \mathbf{h}) U(\mathbf{h})\,. \tag{5}$$

Suppose that we already know the phases on the right hand side of Eq. (5) but not on the left; we can generate the phase for $U(\mathbf{k})$ straightforwardly — this is known as phase extension. Alternatively Eqs. (4) and (5) represent a set of self-consistency equations that the correct phases have to obey. For $M$ unknown phases there are $M$ equations of the form of (5); so, in principle, the problem is completely solved.

With real experimental data the situation is not so simple; there are measurement errors and not all the structure factors may have been measured. In addition, not all the atoms are the same. More rigorously, the "equal" signs above should be replaced by the "probably equal" sign $\approx$, but the same concepts hold. Crystallographic Direct Methods find plausible solutions for the phases which are self-consistent in some sense, with the degree of self-consistency measured by some Figure of Merit (FOM). Rather than just finding one solution, a set of plausible solutions is considered, and the corresponding real-space forms called "maps." It may only be necessary to consider the solution with the best FOM and the map may approach a true restoration of the phases (and real-space charge density). In other cases (which will be discussed below) not all the phases will be correct but among the top solutions there will be enough of the correct sites that the rest can be found. While our experience is that the maps are generally exceedingly good, approaching restorations, it is better to be conservative about their interpretation:

(a) Not all the peaks are in exactly the right places for the atoms, but are off by 0.1–0.2 Å;
(b) The heights of the peaks may be incorrect;
(c) There may be too few or too many peaks.

However, these maps represent a set of plausible models for the structure against which to do a more rigorous refinement.

For a good set of three-dimensional measurements including all reflections to atomic scale resolution (1.0–1.5 Å), the problem of obtaining solutions is (probably) more limited by available computer power than anything else. A surface represents a special case, in either two or three dimensions. To understand this, it is important to discriminate between what, in a LEED notation, are called the fractional order reflections versus the integer order reflections. While the top atomic layers with positions different from the bulk contribute substantially to the first, for the integer orders there are large contributions from the bulk atoms. One cannot sensibly extract the structure factor for these integer reflections when it is superimposed on this typically far larger bulk signal. While there are strategies being developed both here and elsewhere to overcome this issue, for the purpose of this paper we will consider these as reflections for which both the amplitude and the phase of the structure factor are unknown. A second problem, one familiar to surface scientists (but not crystallographers), is that one has only a very poor idea of how many atoms there are in the unit cell. For some material A on a substrate B, the number of A atoms might be known to an accuracy of 20%, but the number of B atoms could be almost anything — this is of course an even more substantial issue in a native reconstruction. Most available programs use the number of atoms as an input parameter and find chemically reasonable arrangements (using typical interatomic distances and bond angles, for instance), which is again not going to be the same for a surface. Related to this, given an initial fragment, say 50% of the atoms, there are a number of classical methods for finding the rest based upon comparing the experimental and calculated intensities. With a surface there can be a substantial fraction of the diffracted intensity arising from small subsurface relaxations; this is not accounted for in classical methods. As a consequence finding the remaining atoms is not so simple and at present requires manual

intervention; doing this in an automated fashion in the future is a challenge.

Of the surface data problems, the most severe is the missing reflections. One can understand their effect via some simple arguments using an approach similar to Eqs. (1)–(5). Let us subdivide the true $u(\mathbf{r})$ into two parts: $u_m(\mathbf{r})$ for the measured reflections and $u_h(\mathbf{r})$ for the unmeasured reflections or holes in the data. We can now write

$$\begin{aligned} u_m(\mathbf{r}) + u_h(\mathbf{r}) &= N\{u_m(\mathbf{r}) + u_h(\mathbf{r})\}^2 \\ &= N\{u_m(\mathbf{r})^2 + 2u_m(\mathbf{r})u_h(\mathbf{r}) \\ &\quad + u_h(\mathbf{r})^2\}\,. \end{aligned} \tag{6}$$

Considering just the measured reflections in reciprocal space as $U_m(\mathbf{k})$,

$$\begin{aligned} U_m(\mathbf{k}) = N \sum_{\mathbf{h}} U_m(\mathbf{k}-\mathbf{h})U_m(\mathbf{h}) \\ + N \sum_{\mathbf{h}} U_m(\mathbf{k}-\mathbf{h})U_h(\mathbf{h})\,, \end{aligned} \tag{7}$$

assuming that the unmeasured reflections form a separate lattice. If the unmeasured reflections are small, the second term on the right can be safely neglected; if they are large it cannot be. What often happens in practice is a Babinet solution,[33] i.e.

$$u(\mathbf{r}) = u_h(\mathbf{r}) - u_m(\mathbf{r})\,, \tag{8}$$

as can be shown by looking at the roots of the quadratic in (6) when $u_h(\mathbf{r})$ is large. This can often be recognized by negative regions which look like atoms when only the measured set is considered.

For a surface we therefore have some set $M_m$ of measured reflections, and another set $M_h$ of unmeasured reflections. This gives us a total of $M_m + 2M_h$ unknowns but only $M_m$ equations. Classical Direct Methods assume that all the strong reflections have been measured and only consider relationships between the measured reflections. (In effect, unmeasured reflections are taken to have zero intensity.) As a consequence they will (probably) fail completely if there are large, unmeasured reflections. What is needed instead are methods which in some fashion include estimates for the unmeasured reflections and/or work when there are not enough equations for a formal mathematical solution. Fortunately such methods already exist, and use the idea of exploiting the entropy as a functional. The best-developed of these is the "Maximum Entropy Method,"[34–44] which maximizes the entropy $S$ given as

$$S = -\sum_{\mathbf{r}} u(\mathbf{r})\,\ln\{u(\mathbf{r})\} \tag{9}$$

summed over the map in real space, coupled with a constraint that the set of $U_m(\mathbf{k})$ values generated have moduli close to that of the experimental data. In effect they interpolate values for the unknown set $U_h(\mathbf{k})$, which gives a real-space form that maximizes the entropy. The approach we have developed[45] is similar, and minimizes the relative entropy[46] given by

$$S_r = \sum_{\mathbf{r}} [u(\mathbf{r})\,\ln\{u(\mathbf{r})/e\langle u(\mathbf{r})\rangle\} + \langle u(\mathbf{r})\rangle]\,. \tag{10}$$

The maximum of Eq. (9) with no other information is when $u(\mathbf{r}) = \langle u(\mathbf{r})\rangle$, which minimizes (to zero) the relative entropy of Eq. (10) for all values of $\mathbf{r}$. Both of these are highly nonlinear and as a consequence have an in-built interpolation of the unmeasured reflections. The fact that the minimum of Eq. (10) is zero has some algorithmic advantages, in that we can use an iterative series solution where an updated estimate is generated from the $n$th estimate via the equation

$$\begin{aligned} u_{n+1}(\mathbf{r}) &= u_n(\mathbf{r})\,\ln\{u_n(\mathbf{r})/\langle u(\mathbf{r})\rangle\} \quad & u_n(\mathbf{r}) > 0 \\ &= 0 & u_n(\mathbf{r}) < 0 \end{aligned} \tag{11}$$

[skipping the last term on the right of Eq. (10) since we are not matching the mean], and the FOM is a measure of how close the relative entropy is to zero for the measured reflections:

$$\mathrm{FOM} = \sum_{\mathbf{k}}{}' |U_n(\mathbf{k}) - \alpha U_{n+1}(\mathbf{k})| / \sum_{\mathbf{k}}{}' |U_n(\mathbf{k})|\,, \tag{12}$$

with $\alpha$ a scalar chosen to minimize (12) and the prime notation indicating that $U(\mathbf{0})$ is excluded from the summations. Ideally the FOM will be zero for the correct solution; in general it is small, in the range of 0.1–0.2. To strengthen the algorithm, we define the unitary structure factors a little differently via

$$U(\mathbf{k}) = W(\mathbf{k})F(\mathbf{k})/\langle f(\mathbf{k})^2\rangle^{1/2}\,, \tag{13}$$

with the window $W(\mathbf{k})$ chosen to satisfy (after Fourier-transforming to real space)

$$w(\mathbf{r}) = \beta w(\mathbf{r})\,\ln\{w(\mathbf{r})/\langle w(\mathbf{r})\rangle\}\,, \tag{14}$$

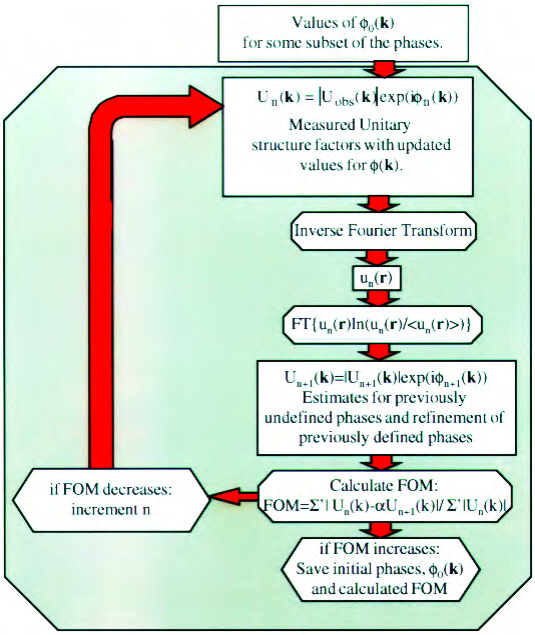


Fig. 1. Flow diagram of the Minimum Relative Entropy algorithm. Initial phase values are controlled by the Genetic algorithm for a global search; for the final calculation the best solutions found are used as input and the final phases stored to produce the maps.

where $\beta$ is a scalar. In effect this builds in a pattern recognition element such that the relative entropy is identically zero for a set of nonoverlapping identical atoms (see next section for a better description). A flow diagram for the whole process is shown in Fig. 1. One useful extension of the above which is effective in many cases is to add in some fragment or estimate of the structure if this is already known. If $e(\mathbf{r})$ is this estimate, and retaining Eqs. (12) and (13) for the FOM calculation an effective iteration process is to use

$$\begin{aligned} u_{n+1}(\mathbf{r}) = u_n(\mathbf{r})\ \ln\{u_n(\mathbf{r})/\langle u(\mathbf{r})\rangle\} \quad & u_n(\mathbf{r}) > 0 \\ +\lambda e(\mathbf{r})\ \ln\{e(\mathbf{r})/u_n(\mathbf{r})\} & \\ = \lambda e(\mathbf{r})\ \ln\{e(\mathbf{r})\} \quad & u_n(\mathbf{r}) < 0\,, \end{aligned} \tag{15}$$

where $\lambda$ is in principle a Lagrangian multiplier, although setting it to one seems to be best. In effect, this incorporates atoms into the structure at the positions of the initial fragment.

A very useful property of this algorithm is that it will automatically generate values for the unmeasured reflections. While originally we did not use these, setting them to zero after each cycle, it has become apparent recently that these interpolated values are in fact quite good. (Why this is the case will become clearer in the next section.) Unfortunately, at least in two dimensions, we have not been able to achieve substantive extrapolation to larger reciprocal lattice vectors (superresolution) while simultaneously determining the phases; to date the algorithm is unstable. Connected to this, the problem of Babinet solutions can often be solved rather simply using the interpolated values. In the first pass one generates stable values for the unmeasured reflections, then flips the phase for the measured reflections by 180° to explore the possibility of a Babinet solution with a better FOM in a second pass.

Such complicated mathematical methods are not always needed, and sometimes structures can be solved very easily. In many cases there are less than $M$ unknown phases since a simple translation of the unit cell cannot change the contents. Except when there are threefold rotational axes, one or more phases can be arbitrarily specified to eliminate simple translations. Further restraints are possible. For instance, based upon the requirement that $u(\mathbf{r})$ be positive, constraints can be set via Determinants connecting different phases.[47] There is also what is known as the $\Sigma_2$ relationships,[48,49] which state that for two reflections $\mathbf{k}$–$\mathbf{h}$ and $\mathbf{h}$, the phase of $\phi(\mathbf{k})$ for reflection $\mathbf{k}$ is given by

$$\phi(\mathbf{k}) \approx \phi(\mathbf{k}\text{–}\mathbf{h}) + \phi(\mathbf{h})\,, \tag{16}$$

with a probability of

$$P(\phi(\mathbf{k})) = \exp(K(\mathbf{k}\text{–}\mathbf{h},\, \mathbf{h})\ \cos(\phi(\mathbf{k}))/2\pi I_0(K(\mathbf{k}\text{–}\mathbf{h},\, \mathbf{h}))\,. \tag{17}$$

with

$$K(\mathbf{k}\text{–}\mathbf{h},\, \mathbf{h}) = 2/\sqrt{N}|E(\mathbf{k})E(\mathbf{k}\text{–}\mathbf{h})E(\mathbf{h})|\,, \tag{18}$$

and the normalized structure factors are defined as

$$E(\mathbf{k}) = F(\mathbf{k})/\{\varepsilon(\mathbf{k})\sqrt{N}\langle f(\mathbf{k})\rangle\}\,, \tag{19}$$

and $\varepsilon(\mathbf{k})$ is a statistical weighting[50] that depends upon the class of a given reflection in the space group. Often the right hand side of Eq. (16) must be 360° (or 180° when glide planes are present). However, since we only have a probability, it is dangerous to rely too much on these. With a few reflections specified to fix the origin and a few others set as variables, one may be able to set up a set of

relationships (called Symbolic Logic[51]) to determine the structure on the back of an envelope — two examples will be given later for the Si(111)-$(7 \times 7)$ and Au on Si(111)-$(\sqrt{3} \times \sqrt{3})$ surfaces.

As a final point, it should be noted that nowhere in the above description has anything been said about whether the data is two-dimensional or three-dimensional. In fact, three-dimensional data tend to be rather easier since the number of terms in the convolution of Eq. (5) is larger and for some special reasons that will be discussed below. However, for almost any surface the $(0, 0, \ell)$ reflections ($z$ normal to the surface) will be rather large and also depend upon surface roughness. To date this does not appear to be a limitation although it is a concern (see also next section).

The final component of any solution method is a way to perform a global search to identify the set of plausible solutions — remember, we are not interested in the absolute minimum but the set of local minima. Many methods exist in the literature, the most common being assigning random phases,[52] a systematic set of encoded phases for certain reflections using what are called "magic numbers,"[53] error-correcting codes[54] or simulated annealing.[55,56] We have used a slightly different approach based upon a genetic algorithm.[57,58] A subset of the phases is selected and these phases are digitized into a binary representation, with typically three bits (eight values)representing a general phase which can be anywhere from 0° to 360°. The bits for each phase (gene) are arranged into a string (chromosome) which represents one individual, and used as starting values for a calculation. For a population of such individuals the FOM is evaluated. These individuals now act in pairs as parents of a new generation of children using cross-linking to produce the new children (see Fig. 2), with a weak weighting to prefer parents with better (smaller) FOM's. The FOM for each of these children is now evaluated, and then they are used to produce the next generation. This rather simple-sounding algorithm has some very powerful convergence properties due to what is called the Schema Theorem.[57] In effect, if we produce $N$ children from $N$ parents, $N^2$ phase combinations are explored for only $N$ FOM calculations. While some care has to be taken to adapt the algorithm such that it will find multiple solutions, rather than just one local minimum, in practice it works rather well and is much faster than a random search.

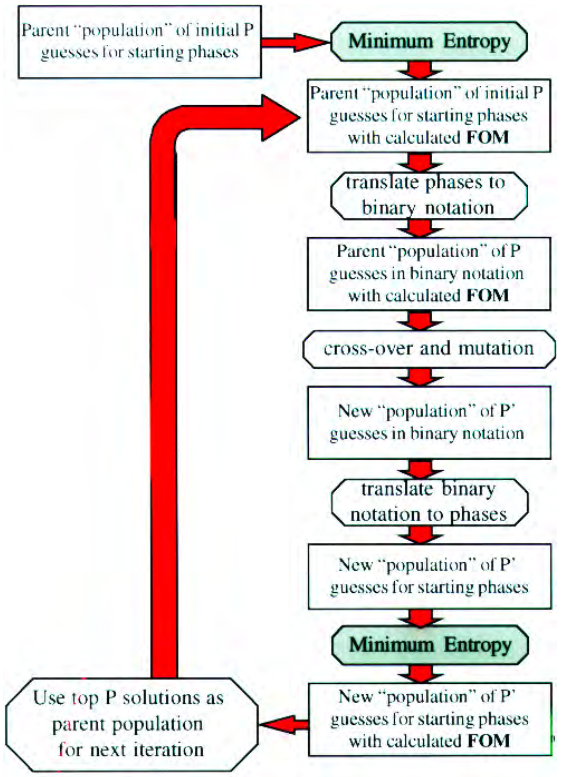


Fig. 2. Flow diagram of the Genetic algorithm routine. "Minimum Entropy" operation refers to the flow diagram shown in Fig. 1.

## 2.2. *Projection onto Sets*

A number of methods have been developed for solving the phase problem for images, parallel with but independent of Direct Methods. These include some mathematical results which are relevant to surface problems. The basic idea is to use sets, and what is called projection onto sets.[27] We consider a set to be those values which satisfy certain conditions or constraints. The set is termed convex if all points on the line connecting any two members are also members, and nonconvex if they are not. In a similar fashion, the constraints which determine the character of a given set can be called convex or nonconvex. A projection operator is defined to be the operation which converts from one set to another. The mathematical theory combining convex, nonconvex sets and iterative projection between sets is called "Projection onto Sets" and can be used to analyze some facets of Direct Methods.

Turning to the specific problem herein, we know the amplitudes of the measured $|U(\mathbf{k})|$ unitary structure factors; our problem is to find the phases $\phi(\mathbf{k})$, such that

$$U(\mathbf{k}) = |U(\mathbf{k})| \exp(i\phi(\mathbf{k}))\,. \tag{20}$$

Let us consider the set of all possible values of $U(\mathbf{k})$, $S_1$, which satisfies the above constraint on the moduli. This set $S_1$, is not convex, but the related set where the phases are known (but not the moduli) is convex. Let the projection operator $P_1$ convert the set $S_1$ to a second set $S_2$, for instance the set of all possible maps which are positive at all points, a convex set. Let $P_2$ be the corresponding projection operator from the set $S_2$ back to the set $S_1$. The iterative sequence

$$U_{n+1}(\mathbf{k}) = P_2 P_1 U_n(\mathbf{k}) \tag{21}$$

attempts to solve for the unknown $U(\mathbf{k})$ using the method of projection onto sets. If the two sets $S_1$, and $S_2$, are both convex, the algorithm is known to converge to the intersection of the two sets. Such convergence is not guaranteed with nonconvex sets, but the iteration is known to normally have an error-reducing property, moving towards the true solution if a good initial set of values is provided.

Direct Methods use for the (forward) projection $P_1$, a set of constraints which are consistent with the fact that the scattering comes from atoms; the (back) projection $P_2$, corrects the amplitude; structure completion methods use different types of projections. (At a formal mathematical level, pure projections are not used; instead a single iteration step is employed.) Using Fourier transforms generic Direct Methods can be represented using the block diagram of Fig. 3, or in terms of sets in Fig. 4. While the constraint that the real space maps are positive leads (by itself) to a convex set, in general neither the real space nor reciprocal space sets are convex. As such they are exceedingly similar to some image restoration algorithms, particularly the Gerchberg–Saxton[59] and Fienup[60,61] algorithms.

Different flavors of Direct Methods use different projection operators and constraints. For instance, classical Direct Methods project the phases using probabilistic relationships ($P_1$) and correct the moduli ($P_2$) iteratively. Maximum Entropy projects the solution onto maxima of the entropy in real space

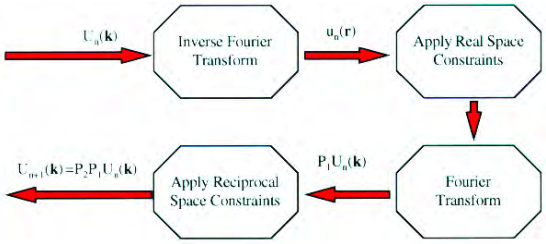


Fig. 3. Block diagram description of Direct Methods in the most general case.

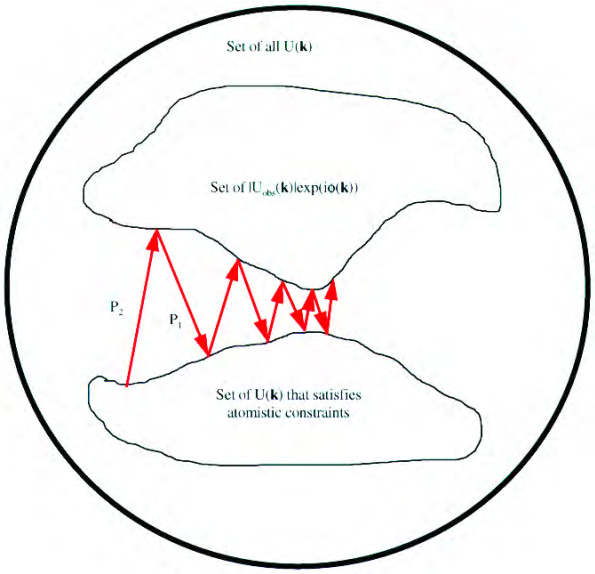


Fig. 4. Illustration of the Projection onto Convex Sets for $U_{n+1}(\mathbf{k}) = P_1 P_2 U_n(\mathbf{k})$ considered for the space of all $U(\mathbf{k})$. The calculated FOM corresponds to the distance along the projection $P_1$.

($P_1$) and the moduli in a $\chi^2$ sense in reciprocal space ($P_2$). The algorithm we use can be written as

$$P_1 : U_{n+1}(\mathbf{k}) = \alpha \mathcal{F}^1\{u_n(\mathbf{r}) \ln\{u_n(\mathbf{r})/\langle u(\mathbf{r})\rangle \text{ if } u(\mathbf{r}) > 0;\ 0 \text{ if } u(\mathbf{r}) < 0\}\,,$$

$$P_2 : |U_{n+1}(\mathbf{k})| = \text{Experimental value}\,,$$

where $\alpha$ is the scaling term from Eq. (12) and $\mathcal{F}^1$ is an inverse Fourier transform. As such it has three components:

(a) The solutions are forced to be positive — a convex constraint.
(b) The solutions are forced to resemble atoms, since identical, independent nonoverlapping atoms are eigensolutions of the minimum relative entropy

treated as an operator. This appears to be a nonconvex constraint.

(c) The moduli are corrected to the experimental values — a nonconvex constraint. The slightly different case where an initial estimate of the structure is available [Eq. (15)] includes a projection onto the set of solutions with atoms at specified locations, the latter a convex constraint. The FOM that we are using is (in the language of Linear Programming) the $L_1$ mean of the distance between the solutions after cycles $n+1$ and $n$ (see Fig. 4), and will be zero for "atomic" solutions matching the experimental data at the intersection of the sets $S_1$ and $S_2$. With measurement error and different atoms the two sets approach, but do not touch, and we find local minimum approach locations.

In terms of the umneasured reflections, if we know their phases and apply the constraint that the solutions are positive, we have two convex sets. From the other reflections a very good estimate of their phases is possible, and it follows that it is mathematically justifiable to expect restoration of the amplitude of the umneasured reflections. (The problem is stability, since the amplitude of the unmeasured reflections affects the phases of the measured reflections.)

An even stronger case can be made with three-dimensional data from a surface. Substantial deviations of the atomic positions exist for only a limited region normal to the surface, and the rel-rods are normally sampled much finer than this. Therefore within the unit cell (whose length normal to the surface is specified by the smallest sampling) the charge density is zero over a large region. This is a strong convex constraint, called in the image restoration literature a support constraint.[62] For a one-dimensional set of $M$ points in real space, with a strong support constraint there are at most $2^M$ unique solution,[63] a substantial reduction compared to the general case ($> 8^M$). (In some cases there is only one solution, but this cannot be predicted in advance.) If the phases for the unmeasured reflections are adequately determined by the other reflections, the one-dimensional problem of determining their amplitudes is completely unique with a support constraint, assuming no axis of symmetry or antisymmetry. It follows that not all the relrod data need to be available for a viable solution to be achieved, even the strong $(0,0,\ell)$ reflections, and the problem is better-conditioned than a two-dimensional problem.

### 2.3. *Structure completion*

Very dependent upon the data, the results of the initial Direct Methods analysis may yield rather accurate locations for $> 90\%$ of the atoms, or only poor estimates for a much smaller number. In practice one does not need much to complete the structure from this initial fragment; knowledge of part of the solution is a strong convex constraint. Many classical methods exist,[64,65] for instance Fourier difference maps based upon the transform of $F_d(\mathbf{k})$, given by

$$F_d(\mathbf{k}) = \{|F_e(\mathbf{k})| - |F_c(\mathbf{k})|\} \exp(i\phi_c(\mathbf{k}))\,, \qquad (22)$$

where $\phi_c(\mathbf{k})$ and $|F_c(\mathbf{k})|$ are respectively the calculated phase and modulus of the structure factor for a given set of atomic positions. Peaks in these difference maps are probable positions for atoms missing from the structure. To date we have rarely found this useful for surface data. More powerful is to build information about atomic positions into the Direct Methods themselves, for instance by using a model as described above. A third approach is to employ what is already known to reconstruct a more complete map, what we have called "heavy atom holography."[7,30] If $F_u(\mathbf{k})$ is the unknown component of the structure factor,

$$\begin{aligned} |F_e(\mathbf{k})|^2 &= |F_c(\mathbf{k}) + f_u(\mathbf{k})|^2 \\ &= |F_c(\mathbf{k})|^2 + 2\,\mathcal{R}e\{F_c(\mathbf{k})^* F_u(\mathbf{k}) + |F_u(\mathbf{k})|^2\,. \end{aligned} \qquad (23)$$

This equation is equivalent to an in-line hologram, and if the known component is reasonably large it can be pseudoinverted in a Wiener filter sense to give

$$F_u(\mathbf{k}) \approx \{|F_e(\mathbf{k})|^2 - |F_c(\mathbf{k})|^2\} F_c(\mathbf{k})^* / \{|F_c(\mathbf{k})|^2 + \delta\}\,, \qquad (24)$$

where $\delta$ is adjustable. (Other pseudoinversion schemes are also plausible.) Feeding this estimate back into Eq. (23) leads to an improved estimate. In general, atom-like peaks in the real-space transform of the unknown component are good estimates for the unknown atomic positions and an iterative procedure can be established as illustrated in Fig. 5.

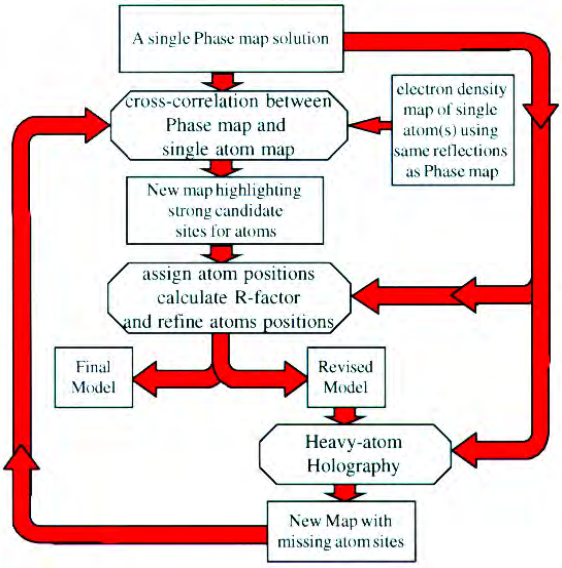


Fig. 5. Flow diagram of iterative procedure using heavy atom holography and refinements to complete a structure.

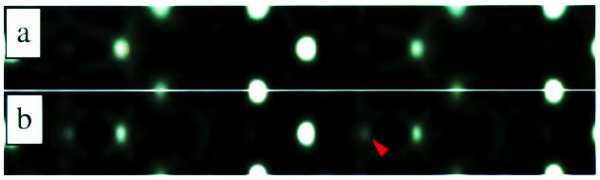


Fig. 6. (a) Scattering potential map for the initial fragment of Si(111)-(4 × 1)/In structure, white being high potential, black low. The fragment consists of two In atoms (center) and two Si atoms in the unit cell. (b) Heavy atom restoration showing the location (arrowed) of an additional Si site.

As an example, Fig. 6(a) shows an initial fragment with two In atoms and two Si atoms from the In on Si(111)-(4 × 1) structure.[24] The heavy atom restoration [Fig. 6(b)] clearly shows one of the silicon atoms needed to complete the structure. While these methods work it would be accurate to state that too much user intervention is required at the current moment and less biased automated methods are needed.

## 2.4. *Refinement*

The final test of any model is to refine the atomic positions against the experimental data. To be rigorous, if we have a set of experimental structure factor moduli $|F_e(\mathbf{k})|$ and calculate a set of values $|F_c(\mathbf{k})|$ we first determine (from the experimental data) the probability distribution of the errors and then refine the negative logarithm of this probability distribution — a maximum likelihood method. Many different functions exist in the literature for different assumptions about the probability distribution, the most common being the $\chi^2$ estimator based upon Gaussian error statistics for the intensities:

$$\chi^2 = 1/(M-V)\sum_{\mathbf{k}}\{|F_e(\mathbf{k})|^2 - \alpha|F_c(\mathbf{k})|^2\}^2/\sigma(\mathbf{k})^2\,, \tag{25}$$

where $M$ is the number of measurements, $V$ the number of variables, $\alpha$ a variable and $\sigma(\mathbf{k})$ the errors in $|F_e(\mathbf{k})|^2$. If the errors are Poisson in character one can approximate

$$\sigma(\mathbf{k}) \approx \text{const}^*|F_e(\mathbf{k})| \approx \text{const}^*|F_c(\mathbf{k})| \tag{26}$$

and reduce this to the equivalent form

$$R^2 = \sum_{\mathbf{k}} \|F_e(\mathbf{k})| - \alpha|F_c(\mathbf{k})\|^2 / \sum |F_e(\mathbf{k})|^2\,. \tag{27}$$

A danger of these is that the errors are rarely Gaussian in character and it is not unusual to have a few outlier points very poorly measured. A good alternative is to use what are called Robust methods, which are less sensitive to these outliers; for instance a double-sided exponential or Laplacian error distribution leading to

$$\chi = 1/(M-V)\sum_{\mathbf{k}} \|F_e(\mathbf{k})|^2 - \alpha|F_c(\mathbf{k})|^2|/\sigma(\mathbf{k}) \tag{28}$$

and the "Crystallographic $R$ factor" assuming Poisson statistics for the errors:

$$R = \sum_{\mathbf{k}} \|F_e(\mathbf{k})| - \alpha|F_c(\mathbf{k})\| / \sum |F_e(\mathbf{k})|\,. \tag{29}$$

[The similarity of the FOM used for the Direct Methods to Eq. (29) is deliberate.] With transmission electron diffraction data a parallel measurement of all the intensities takes seconds, so a number of independent measurements can be made. By treating these as repeat measurements the error distribution can be determined as illustrated in Fig. 7. For X-ray diffraction each measurement takes much longer, so determining the random (and systematic) errors is harder. Evidence to date indicates that TED errors are close to Gaussian/Poisson distributions, but those in X-ray measurements are not and scale closer to

$$\sigma(\mathbf{k}) \approx \text{const}^*|F_e(\mathbf{k})|^2 + \text{background}\,. \tag{30}$$

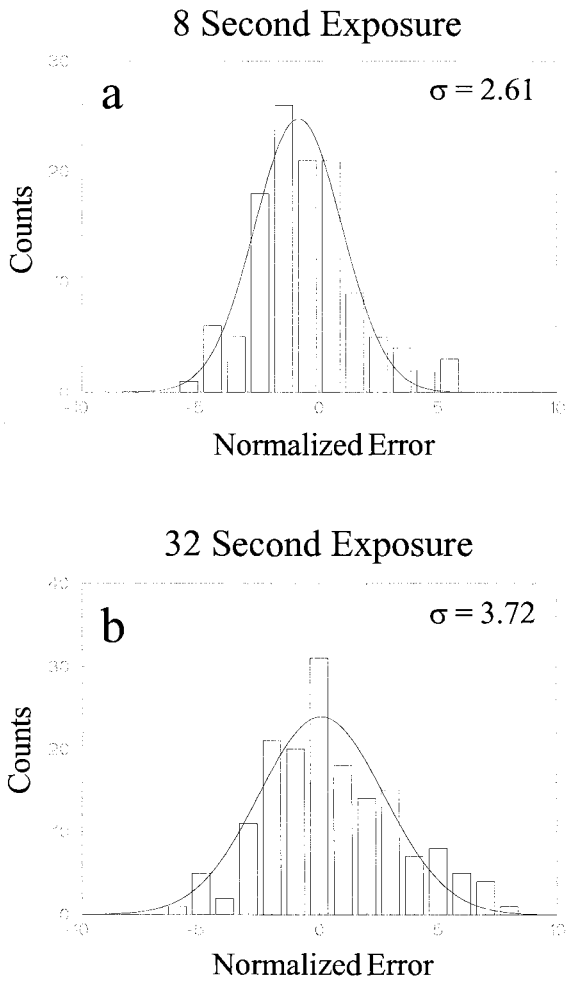


Fig. 7. Distribution of measurement errors for two different TED negatives from the same data set. (a) From negative exposed for 8 s. (b) From negative exposed for 32 s. The normalized error is defined for each intensity as: [(measured value for intensity on negative) − (average value from entire data set for intensity)]/[measured value for intensity on negative]$^{1/2}$. Gaussian curves have been fit to each distribution. The standard deviation for the longer exposure negative is higher due to increased background signal.

For a complete analysis it is necessary to include subsurface relaxations which can have substantial effects, and for TED the weaker (but important for refinement) scattering by the substrate. To prevent nonphysical atomic displacements from occurring it is possible to constrain these via some interatomic potential, for instance a Keating potential. An alternative is to expand the subsurface displacement field $\mathbf{R}(\mathbf{r})$ as decaying biharmonics which satisfy the equations for isotropic, inhomogeneous elasticity,[66,67] the simplest of which is

$$\mathbf{R}(\mathbf{r}) = \nabla \sum_{\mathbf{g}} [A_g \cos(2\pi \mathbf{g}\cdot\mathbf{r}) + B_g \sin(2\pi \mathbf{g}\cdot\mathbf{r})] \exp(-2\pi g z)\,, \quad (31)$$

where the summation is over the two-dimensional reciprocal lattice vectors $\mathbf{g}$ of the reconstructed cell, and $A$, $B$ constants varied in the fitting procedure.

## 3. Crystallographic Surface Crystallography

It is very common to describe surfaces in terms of LEED notation using the primitive $1 \times 1$ lattice as the starting point, so reciprocal lattice points have fractional indices.[68] In any (conventional) crystallography the symmetry of the unit cell plays a crucial role for symmetry-equivalent reflections, constraints on the phases and also a number of statistical relationships.[50] As an example, the Woods notation of $\sqrt{3} \times \sqrt{3}$R30 on a (111) surface is highly ambiguous; the symmetry could be p3 (twinned), p3ml, p3lm, p6 or p6mm — which of these is correct matters not only for structure refinement but also for other properties, such as the electronic and phonon structure. It is also more conventional to reference reciprocal lattice vectors to the large unit cell, avoiding fractional indices. For these reasons the case is made here that it is better to use the standard notations that can be found in the International Crystallography Tables,[69] conforming to the rest of the crystallographic community. Since there is no possible symmetry above and below the plane of the surface, the number of plane groups is rather limited, summarized in Table II together with the full, three-dimensional space groups. Included in the table are the alternate descriptions for the rectangular unit cells which correspond to switching the relative orientation of the axes and symmetry elements; for instance, it is easier to consider that a $4 \times 1$ unit cell is p1m1 or p11m rather than switching between $4 \times 1$ and $1 \times 4$ cells with pm symmetry.

## 4. Experimental Examples

### 4.1. *Si(111)-(7 × 7)*

The silicon (111) $7 \times 7$ surface is a good test system for Direct Methods. On one hand it is rather simple

Table II. Possible two-dimensional plane groups with their short, full and alternative settings as well as the three-dimensional space group. For completeness, P1a1 is equivalent to p11g; the other setting is not shown in detail in the current tables.

| System | Point group | Symbol | | | 3D | |
|---|---|---|---|---|---|---|
| | | Short | Long | Alternate | | |
| Oblique | 1 | | p1 | | P1 | #1 |
| | 2 | | p2 | | P112 | #3 |
| Rectangular | m | pm | p1m1 | p11m | P1m1 | #6 |
| | | pg | p1g1 | p11g | P1a1 | #7 |
| | | cm | c1m1 | c11m | C1m1 | #8 |
| | 2mm | | p2mm | | Pmm2 | #25 |
| | | | p2mg | p2gm | Pma2 | #28 |
| | | | p2gg | | Pba2 | #32 |
| | | | c2mm | | Cmm2 | #35 |
| Square | 4 | | p4 | | P4 | #75 |
| | 4mm | | p4mm | | P4mm | #99 |
| | | | p4gm | | P4bm | #100 |
| Hexagonal | 3 | | p3 | | P3 | #143 |
| | 3m | | p3m1 | | P3m1 | #143 |
| | | | p31m | | P31m | #157 |
| | 6 | | p6 | | P6 | #168 |
| | 6mm | | p6mm | | P6mm | #183 |

since it is essentially p6mm, and so the phases are either 180° or 360°. (The true symmetry is p31m but the deviation from p6mm is small.) What makes it hard is that the structure factor for the $\{7,7\}$ reflections is three to four times larger than that of any of the other reflections, coincident with a bulk (220) reflection and therefore unmeasurable. Consequently the structure is very difficult to solve except by methods that have an interpolation component.

#### 4.1.1. *Symbolic Logic*

One of the first methods we used[23] was symbolic logic.[51] A very large number of the strong reflections have a $\Sigma_2$ relationship suggesting not only that the $(7,7)$ reflection is strong but that it is 360° (see Fig. 8). Furthermore, reflections connected by any vector in the family $\{7,7\}$ are probably the same provided that they are strong, i.e.

$$\varphi(6,\,1) \approx \varphi(8,\,0)\,, \tag{32}$$

$$\varphi(7,\,1) \approx \varphi(0,\,6)\,. \tag{33}$$

There are also $\Sigma_2$ relationships suggesting that $(0,13)$ is 360°, and strong $\Sigma_2$ relationships (with symmetry-related values) that

$$\varphi(6,\,1) + \varphi(7,\,7) \approx \varphi(13,\,0)\,, \tag{34}$$

so

$$\varphi(6,\,1) + \varphi(8,\,0) \approx \varphi(0,\,13) \approx 360^\circ\,. \tag{35}$$

Enough is now known that the structure can be solved rather accurately by varying ten additional reflections, with the result shown in Fig. 9.

#### 4.1.2. *Phase extension from an HREM model*

Much easier is the case where some of the phases are already known[23] from another experiment, such as an HREM image.[9] Figure 10(a) shows the initial map excluding the $\{7,0\}$ reflections and Fig. 10(b) the resultant extension. All the atoms in the top three layers are present in the map due to good interpolation of the $\{7,0\}$ and $\{7,7\}$ reflections.

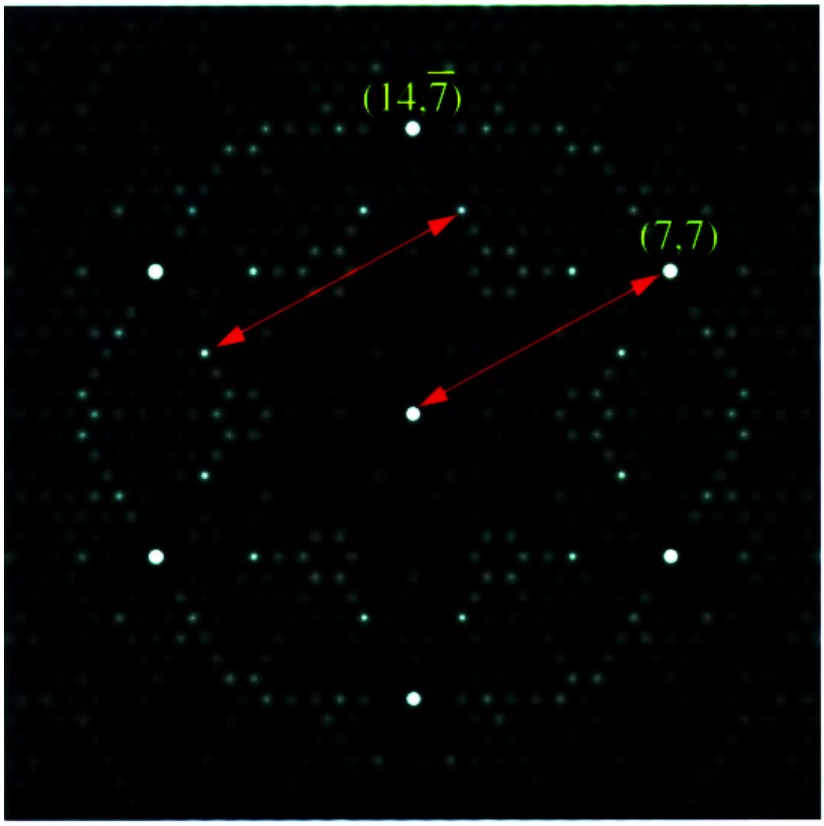


Fig. 8. Modulus of the structure factors using electron diffraction data for the Si(111)-$(7 \times 7)$ surface. The values for the reflections which overlap bulk beams or surface $1 \times 1$ periodicities have been interpolated by the minimum relative entropy method. The $(7, 7)$ reflection is by far the strongest beam. Two red arrows show how the strong $(3, -10)$ and $(10, -3)$ reflections are connected by a $(7, 7)$ vector — since their phases are identical this indicated 360 for $(7, 7)$. Many other pairs of strong reflections connected by $\{7, 7\}$ vectors can be found.

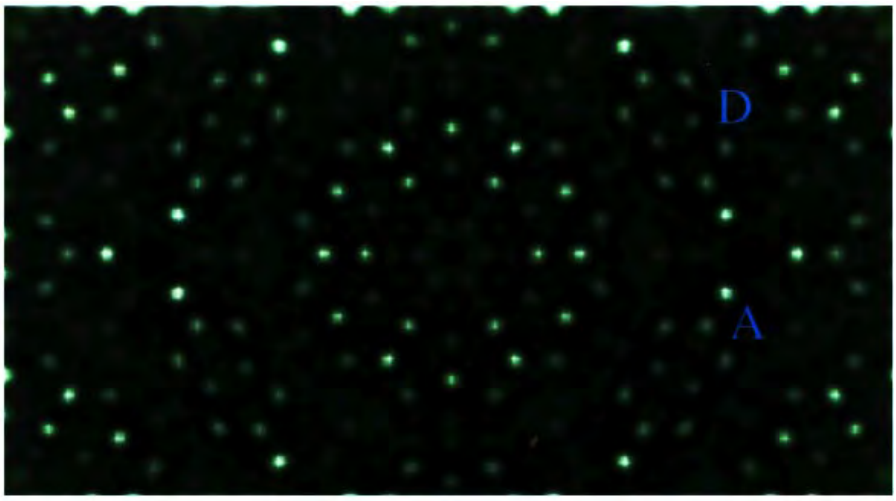


Fig. 9. Map of the scattering potential for the Si(111)-$(7 \times 7)$ surface solved by deriving phase relations for some of the strong beams using symbolic logic and then searching over ten additional reflections with a genetic algorithm. Some artifacts are present in the map due to the small number of reflections used in the search. The dimer sites (D) and the adatoms (A) are marked in the figure.

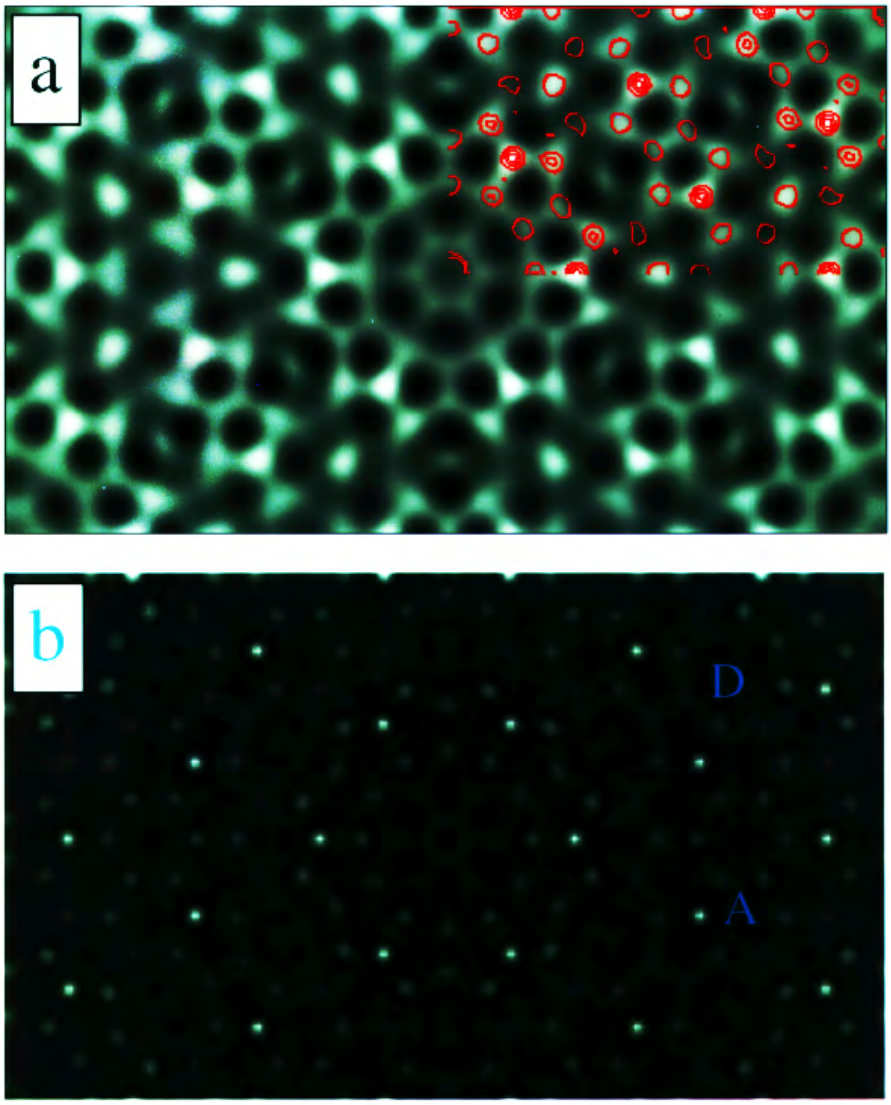


Fig. 10. (a) An initial scattering potential map for the Si(111)-(7 × 7) surface constructed with phases determined from an HREM image [the (7, 0) reflection has been excluded]. Contours of the final 7 × 7 map have been overlaid in the top right corner to highlight the location of the atoms in the structure. (b) The potential map after phase extension, which shows much better definition of the atomic sites than in either Fig. 9 or Fig. 11(a). The dimer sites (D) and the adatoms (A) are marked in the figure.

#### 4.1.3. Ab initio *solutions*

Harder by far is to solve the structure with no prior information — if the {7, 7} reflections are not interpolated a Babinet solution is obtained. This was first done[23] using the Maximum Entropy method, but we have recently been able to solve using the minimum relative entropy approach after stabilizing the interpolation of the unmeasured results. The results are shown in Fig. 11(a). For reference, Fig. 11(b) shows the same phases without the interpolated reflections. The reader should not think that this surface would be solved easily, without any prior information; there are other solutions which would have to be tested in detail.

### 4.2. *Metals on Si(111)*

A very simple example to illustrate solving a structure with little effort is Au on Si(111)-($\sqrt{3} \times \sqrt{3}$).[22]

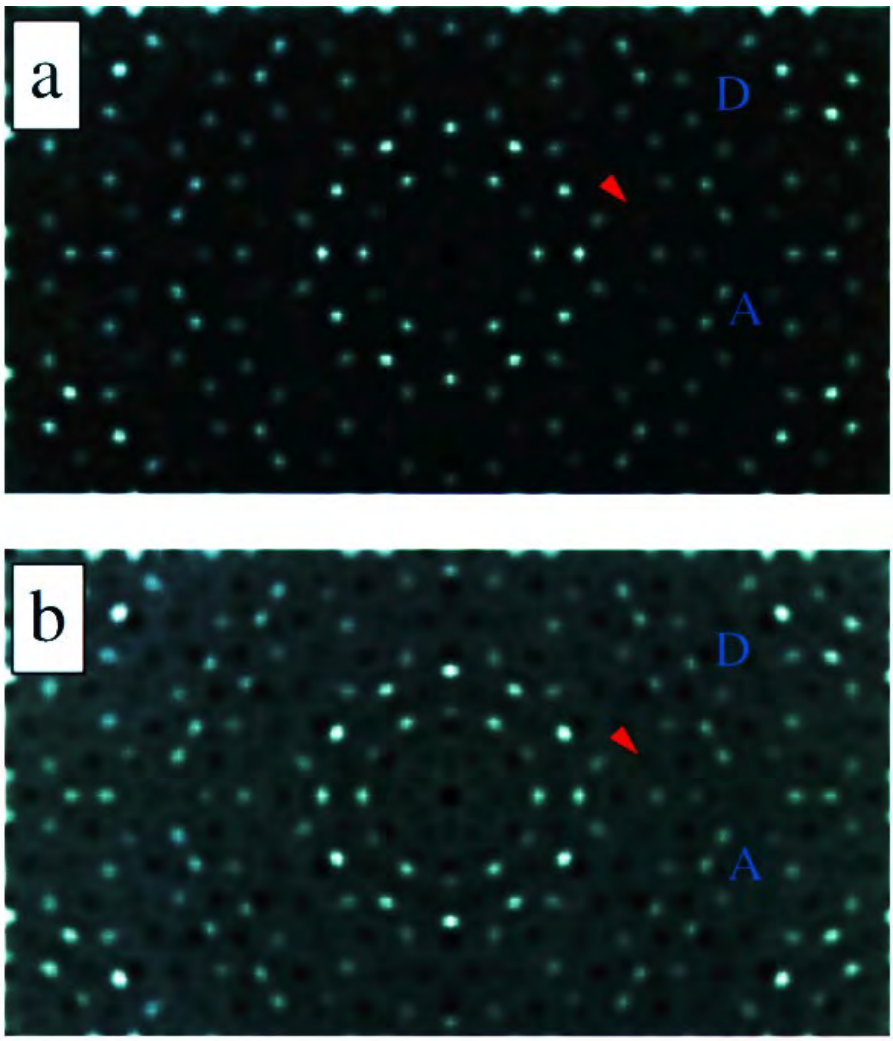


Fig. 11. (a) *Ab initio* solution of the Si(111)-$(7 \times 7)$ structure determined by the minimum relative entropy approach with interpolated estimates for the unmeasured reflections. (b) The same solution without the interpolated reflections. The dark holes are due to the missing reflections, and an arrow indicates the location of one atom that essentially disappears without the interpolated beams. The dimer sites (D) and the adatoms (A) are marked in the figure.

The diffraction data indicate that the $\{2, 1\}$ reflections are far stronger than anything else. Taking the space group as p31m, there is the relationship

$$\phi(2,\,1) \approx \phi(-1,\,3) - \phi(-3,\,2) \approx -2\phi(2,\,1)\,, \quad (36)$$

so

$$\phi(2,\,1) \approx 120n\,, \quad n = 0,\,1\,. \quad (37)$$

The case where $n = 0$ gives just one large peak [Fig. 12(c)], and the coverage is known to be closer to three Au atoms per unit cell. Using just these reflections and $n = 1$ gives the map shown in Fig. 12(b), with the well-known trimer structure. Three other examples using the more complete method described above searching all the reflections are the Ag on Si(111)-$(\sqrt{3} \times \sqrt{3})$ surface[30,71] shown in Fig. 13, the In on Si(111)-$(4 \times 1)$ surface[24] in Fig. 14, and the Ag on Si(111)-$(3 \times 1)$ surface[25] in Fig. 15 — the maps approach restorations.

### 4.3. *Sulfur on metals*

The opposite extreme to a heavy metal on a lighter substrate is a lighter element such as sulfur on a metal. At least in the cases examined to date this has not proved any harder. An example is the S

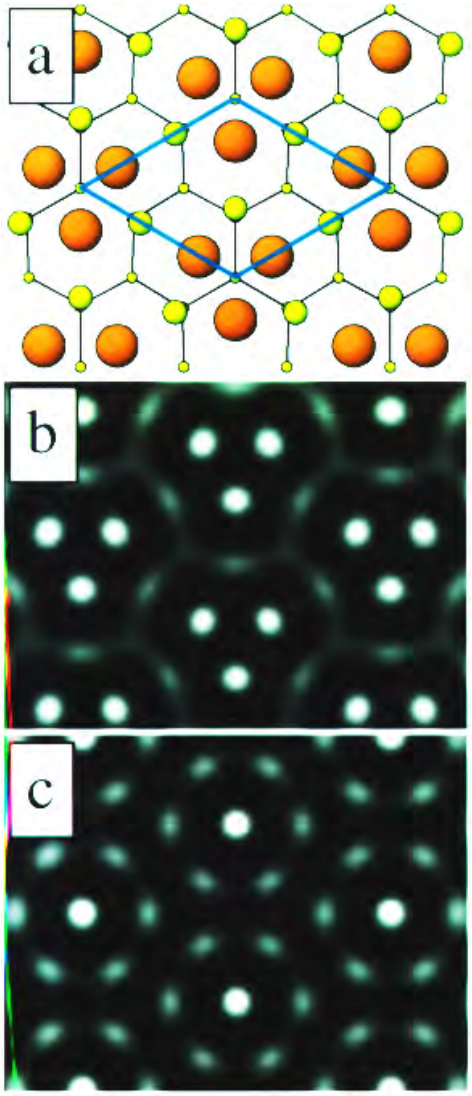


Fig. 12. (a) Accepted model structure for the Au on Si(111)-($\sqrt{3} \times \sqrt{3}$) surface. Gold atoms are orange, silicon is yellow, and the p31m unit cell is outlined in blue. (b) Scattering potential map formed from only the $(2, 1)$ reflection and symmetry-related beams with $\phi(2, 1)$ set to 120°. (c) Scattering potential map formed from only the $(2, 1)$ reflection and symmetry-related beams with $\phi(2, 1)$ set to 0°.

on Ni(111)-($5\sqrt{3} \times 2$) "clock structure"[71] shown in Fig. 16; a second the S on Cu(111) "zigzag"' structure[72] in Fig. 17. In both cases the maps approach restorations.

### 4.4. *Bi on Cu(110)*

A case which illustrates some of the limitations of the method and the role of subsurface strains is Bi on Cu(110).[73] The maps shown in Fig. 18 clearly show the bismuth atoms, but very little about the copper; the bismuth scattering completely dominates that from the lighter copper atoms. Just including these atoms does not completely solve the structure, and additional relaxations to the copper are needed in the final solution.[73]

## 5. What Can Go Wrong?

Many things. The most pathological situation is twinning, and there are cases such as Sn on Si(111),[74] where there is complete overlap of three domains at each reciprocal lattice point. Much simpler twinning, for instance two p1 domains giving an effective pm symmetry, does not appear to be limiting; the maps yield results indicating double-positioning, not too hard to separate at least for simpler structures. Another problem is when two different surface phases give some of the same reciprocal lattice vectors. In some cases one can exclude the perturbed reflections from the data set and obtain viable solutions.

Connected to the above is a more fundamental issue related to the coherence between domains. If one has a random combination of relatively large domains, large compared to the transverse coherence of the (X-ray or electron) beam intensities of the two domains should be added incoherently. However, if the domain size is small compared to the transverse coherence length, in most cases the domain diffraction should be added coherently equivalent to partial occupancies of sites. The reality is probably halfway between these two extremes with partial coherence, and how to determine this and refine appropriately atomic positions remains an unclear issue.

Last but not least, one has the unmeasured reflections. As mentioned before, in practice these can to lead to Babinet solutions which require some care to detect and explore. It seems that this problem is slowly vanishing as we improve the stabilization of our approach, although it is too soon to claim victory.

## 6. Discussion

Direct Methods for bulk structure determination are approaching their 50th anniversary; for surfaces their age is only a year or so. Obviously much more needs to be done and can be done. There are a large

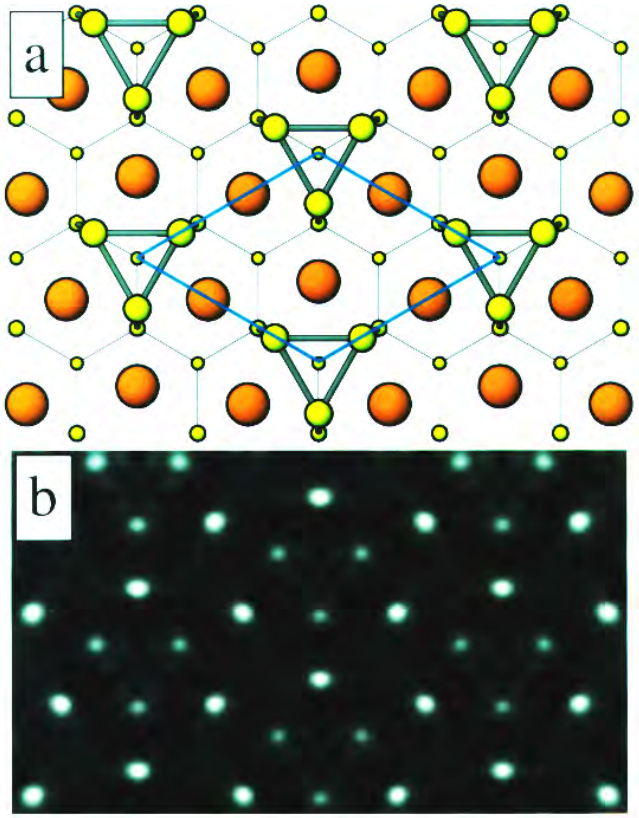


Fig. 13. (a) The honeycomb-chained triangle model for the Ag on Si(111)-($\sqrt{3} \times \sqrt{3}$) surface. Silver atoms are shown in orange, silicon is yellow, and the p31m unit cell is outlined in blue. (b) Phasing map of the scattering potential found from TED data.

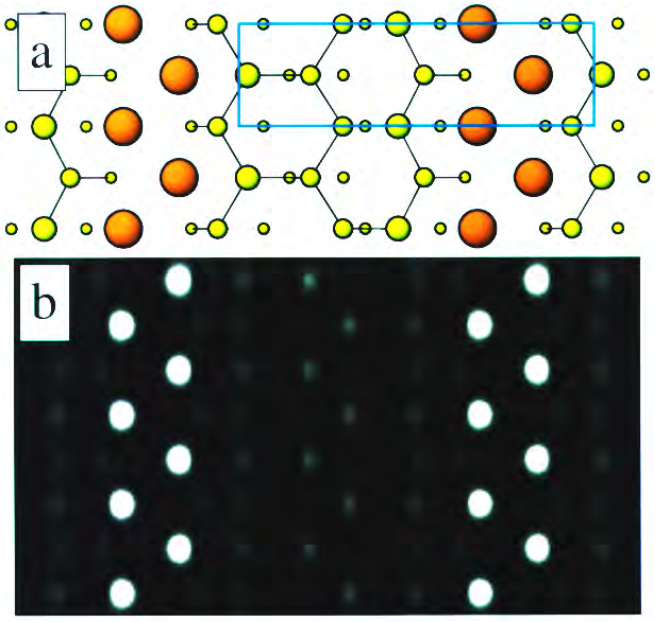


Fig. 14. (a) Model for the In on Si(111)-($4 \times 1$) surface structure. Indium is shown in orange, silicon in yellow, and a pm unit cell is outlined in blue. (b) Direct phasing map of the scattering potential found using TED data. The phasing analysis was done in the p2mg plane group; the true symmetry for the final refinements is pm.

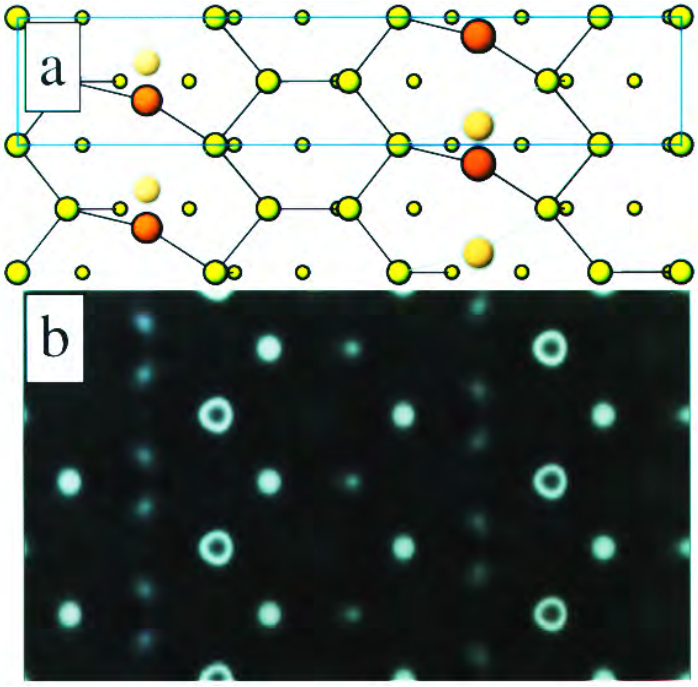


Fig. 15. (a) Model for the Ag on Si(111)-$(3\times1)$ surface structure. Two equivalent, half-occupied silver sites are shown in two shades of orange. The silicon is yellow and a $6\times1$ cm unit cell is outlined in blue. (b) Direct phasing map of the scattering potential calculated from TED data. The structure is p1-twinned to give an effective pm symmetry, so the quality of the map is not as high as in some of the other cases examined to date.

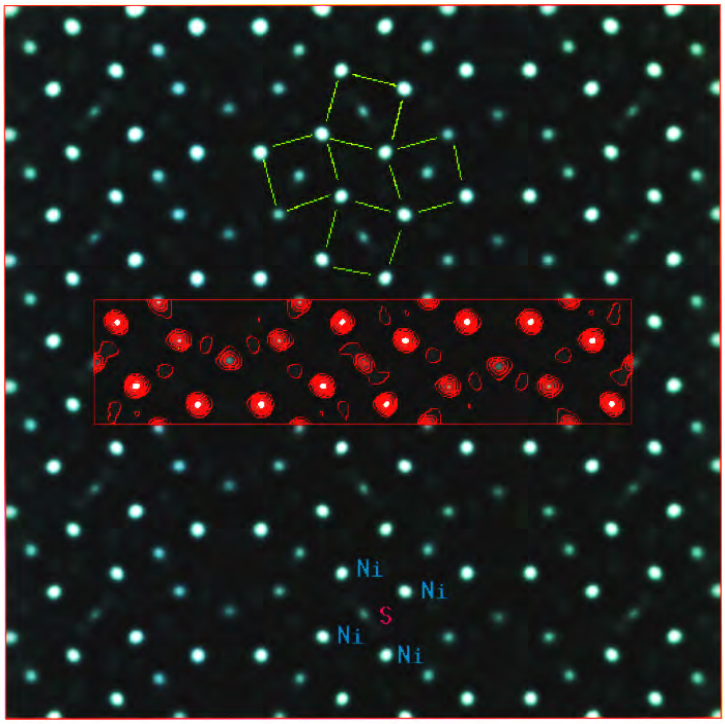


Fig. 16. Charge density map determined for the S on Ni(111)-$(5\sqrt{3}\times2)$ "clock structure," with contours for a single unit cell overlaid. The fourfold arrangement of the Ni atoms around the S atoms is indicated.

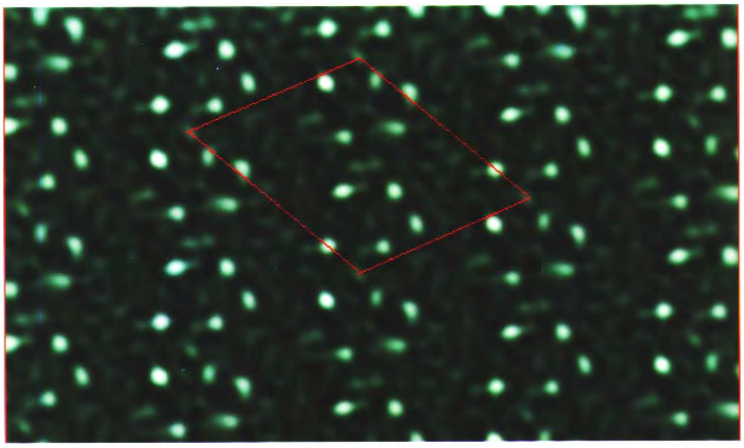

Fig. 17. Charge density map determined for the S on Cu(111) "zigzag" structure, with a single unit cell marked. A similar fourfold arrangement of Cu atoms around the S atoms as in Fig. 16 can be seen. The map is not as symmetric as the published refined structure, suggesting some disorder.

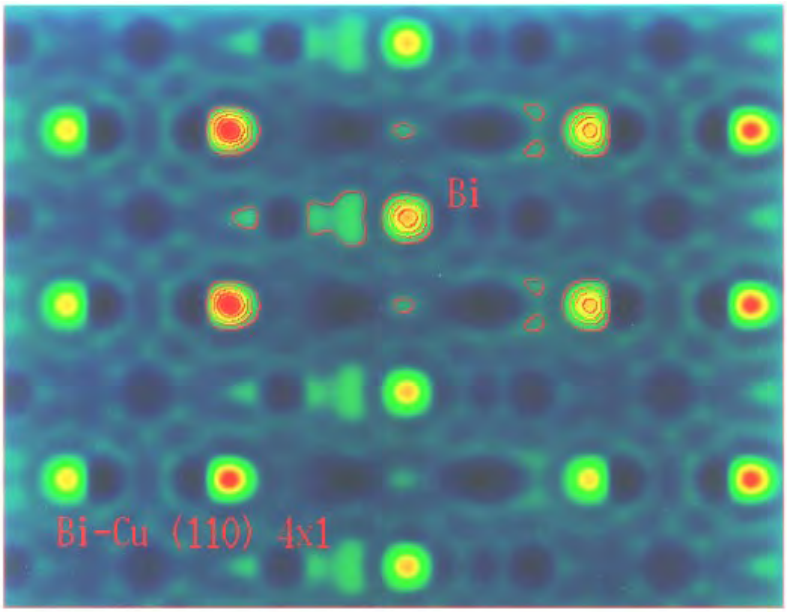


Fig. 18. Charge density map determined for Bi on Cu(110) shown in pseudocolor with red high, blue/black low. The Bi atoms are very clear, with perhaps a hint of the Cu relaxations — for the latter additional structure completion work would be required.

number of literature methods, some of which may translate to the surface problem and prove useful. There may also be ways of exploiting what is known about the missing reflections. One strategy that is being explored is to use the values for a perfect $1 \times 1$ lattice for these, then a heavy atom inversion method; alternatively they could be built into the approaches described herein with some modifications. To what extent Direct Methods for surfaces can become "black-box" methods with little or no user input required is not clear. One can purchase routines for bulk structures and they appear to work very well (in the bulk), but how one can automate issues such as determining registry remains unclear.

Direct Methods are most powerful for larger unit cell structures where Patterson-based techniques

break down and it is impossible to search all the possible alternatives. In two dimensions with a standard workstation the Direct Methods code only takes about 30 min for a reasonable number of beams (100), and a few hours in three dimensions with 1000 reflections. Here the main limitation is obtaining the experimental data. While TED data is much faster to collect, at present there does not seem any simple way to obtain three-dimensional information; here X-ray methods are superior. TED does have certain advantages, most notably a weaker dependence upon the atomic number and much higher sensitivity to charge transfer. Therefore it is more useful for heavy elements on a light substrate and (in principle, albeit to date not in practice) looking for ionicity. A disadvantage is that the kinematical approximation, while good for symmetry-averaged data, is not strictly correct for TED — certainly inadequate for refinements. (To date the maps from TED have not been quite as clean as those from X-ray data, so some weak dynamical effects probably carry over into the phase analysis.) With improvements in sources and detectors large unit cell structures such as Langmuir–Blodgett films or even ordered protein structures should be plausible and not unreasonably expensive in computer time.

## Acknowledgments

The authors are indebted to Dr Fiedenhans'l for the X-ray data sets described herein. We would like to acknowledge the support of the National Science Foundation via grant DMR-9214505 and the support of the Air Force Office of Scientific Research via grants #F49620-94-1-0164 and #F49620-92-J-0250 in funding this work.

## References

1. G. Binning and H. Roher, *Rev. Mod. Phys.* **59**, 615 (1987).
2. L. E. C. van de Leemput and H. van Kempen, *Rep. Prog. Phys.* **55**, 165 (1992).
3. F. Ogletree and M. Salmerón, *Prog. Sol. State Chem.* **20**, 235 (1990).
4. H. Roher, *Surf. Sci.* **299/300**, 956 (1994).
5. S. H. Cohen, M. T. Bray and M. L. Lightbody, *Atomic Force Microscopy/Scanning Tunneling Microscopy* (Plenum, New York, 1994).
6. G. Nihoul, K. Abdelmoula and J. J. Métois, *Ultramicroscopy* **12**, 353 (1984).
7. L. D. Marks and R. Plass, *Phys. Rev. Lett.* **75**, 2172 (1995).
8. G. Jayaram, R. Plass and L. D. Marks, *Interface Sci.* **2**, 379 (1995).
9. E. Bengu, R. Plass, L. D. Marks, T. Ichihashi, P. M. Ajayan and S. Iijima, *Phys. Rev. Lett.* **77**, 4226 (1996).
10. M. M. Woolfson, *Acta Cryst.* **A43**, 593 (1987).
11. C. Giacovazzo, *Direct Methods in Crystallography* (Plenum, New York, 1980).
12. M. M. Woolfson and H. Fan, *Physical and Non-physical Methods of Solving Crystal Structures* (Cambridge University Press, Cambridge, 1995).
13. J. J. Barton, *Phys. Rev. Lett.* **61**, 1356 (1988).
14. J. J. Barton, *J. Electron Spectroscopy and Related Phenomena* **51**, 37 (1990).
15. S. Evans, *J. Electron Spectroscopy and Related Phenomena* **70**, 217 (1995).
16. C. S. Fadley, S. Thevuthansan, M. P. Kaduwela, C. Westphal, Y. J. Kim, R. Ynzunza, P. Len, E. Tober, F. Zhang, Z. Wang, S. Ruebush, A. Budge and M. A. Van Hove, *J. Electron Spectroscopy and Related Phenomena* **68**, 19 (1994).
17. C. S. Fadley, Y. Chen, R. E. Couch, H. Daimon, R. Denecke, J. D. Denlinger, H. Galloway, Z. Hussain, M. P. Kaduwela, J. Y. Kim, P. M. Len, J. Liesegang, J. Menchero, J. Morais, J. Palomares, S. D. Ruebush, E. Rotenberg, M. B. Salmeron, R. Scalettar, W. Schattke, R. Singh, S. Thevuthasan, E. D. Tober, M. A. Van Hove, Z. Wang and R. Ynzunza, *Prog. Surf. Sci.* **54**, 341 (1997).
18. P. M. Len, F. Zhang, S. Thevuthasan, A. P. Kaduwela, M. A. Van Hove and C. S. Fadley, *J. Electron Spectroscopy and Related Phenomena* **76**, 351 (1995).
19. D. K. Saldin, *Surf. Rev. Lett.* **4**, 441 (1997).
20. D. K. Saldin and P. L. De Andres, *Phys. Rev. Lett.* **64**, 1270 (1990).
21. B.P. Tonner, *Ultramicroscopy* **36**, 130 (1991).
22. L. D. Marks, R. Plass, D. L. Dorset, *Surf. Rev. Lett.* **4**, 1 (1997).
23. C. J. Gilmore, L. D. Marks, D. Grozea, C. Collazo, E. Landree and R. D. Twesten, *Surf. Sci.* **381**, 77 (1997).
24. C. Collazo-Davila, L. D. Marks, K. Nishii and Y. Tanishiro, *Surf. Rev. Lett.* **4**, 65 (1997).
25. C. Collazo-Davila, D. Groze and L. D. Marks, *Phys. Rev. Lett.* **80**, 1678 (1998).
26. L. D. Marks, *Phys. Rev. B*, submitted (1998).
27. M. I. Sezan and H. Stark, *Image Recovery: Theory and Application: Applications of Convex Projection Theory to Image Recovery in Tomography and Related Areas*, ed. H. Stark (Academic, Orlando, 1987), pp. 415–462.
28. L. D. Marks, D. Grozea, R. Feidenhans'l, M. Nielsen and R. L. Johnson, *Surf. Rev. Lett.* **5**, 459 (1998).
29. E. Landree, L. D. Marks, P. Zschack and C. J. Gilmore, *Surf. Sci.* **408**, 300 (1998).

30. D. Grozea, E. Landree, C. Collazo-Davila, E. Bengu, R. Plass and L. D. Marks, "Micron: Special Edition," in press (1998).
31. C. Collazo-Davila, D. Grozea, L. D. Mark and R. Feidenhans'l, *Surf Sci.*, submitted (1998).
32. R. Plass, K. Egan, C. Collazo-Davila, D. Grozea, E. Landree, L. D. Marks and M. Gajdardziska-Josifovska, *Phys. Rev. Lett.*, submitted (1998).
33. J. M. Cowley, *Diffraction Physics* (Elsevier, New York, 1990), pp. 48–49.
34. X. Zhuang, E. Østevold and R. M. Haralick, *Image Recovery: Theory and Application: The Principle of Maxiumum Entropy in Image Recovery*, ed. H. Stark (Academic, Orlando, 1987), pp. 157–194.
35. G. Bricogne, *Acta Cryst.* **A40**, 410 (1984).
36. G. Bricogne, *Acta Cryst.* **A44**, 517 (1988).
37. C. J. Gilmore, G. Bricogne and C. Bannister, *Acta Cryst.* **A46**, 297 (1990).
38. G. Bricogne and C. J. Gihnore, *Acta Cryst.* **A46**, 284 (1990).
39. G. Bricogne, *Maximum Entropy in Action*, eds. B. Buck and V. A. Macaulay (Oxford University Press, Oxford, 1991), p. 187.
40. K. Shankland, C. J. Gilmore, G. Bricogne and H. Hashizume, *Acta Cryst.* **A49**, 493 (1993).
41. C. J. Gilmore and G. Bricogne, *Crystallographic Computing 5*: *From Chemistry to Biology*, eds. D. Moras, A. D. Podjarny and J. C. Theirry (Oxford University Press, Oxford, 1993), p. 298.
42. C. J. Gilmore, *Crystallographic Computing 6*: *A Window on Modern Crystallography*, eds. H. D. Flack, L. Parkanyi and K. Simon (Oxford University Press, Oxford, 1993), p. 25.
43. C. J. Gilmore, K. Shanklandrand and G. Bricogne, *Proc. Roy. Soc. Ser.* **A442**, 97 (1993).
44. I. G. Voigt-Martin, D. H. Yan, A. Yakimansky, D. Schollmeyer, C. J. Gilmor and G. Bricogne, *Acta Cryst.* **A51**, 849 (1995).
45. L. D. Marks and E. Landree, *Acta Cryst. A*, in press (1998).
46. T. M. Cover and J. A. Thomas, *Elements of Information Theory* (John Wiley and Sons, New York, 1991).
47. M. M. Woolfson and H. Fan, *op. cit.*, p. 73.
48. U. Shmueli and G. H. Weiss, *Introduction to Crystallographic Statistics* (Oxford University Press, Oxford, 1995), p. 139.
49. J. Karle and H. Hauptman, *Acta Cryst.* **9**, 635 (1956).
50. U. Shmueli and G. H. Weiss, *op. cit.*, pp. 9l–97.
51. M. M. Woolfson and H. Fan, *op. cit.*, pp. 84–87.
52. J. X. Yao, *Acta Cryst.* **A37**, 642 (1981).
53. P. S. White and M. M. Woolfson, *Acta Cryst.* **A31**, 53 (1975).
54. C. J. Gilmore and W. V. Nicholson, *Trans. Am. Cryst. Ass.* **30**, 15 (1994).
55. G. M. Sheldrick, *Acta Cryst.* **A46**, 467 (1990).
56. N. T. Bhat, *Acta Cryst.* **A46**, 735 (1990).
57. D. E. Goldberg, *Generic Algorithm in Search, Optimization, and Machine Language* (Addison-Wesley, Reading, 1989).
58. E. Landree, C. Collazo-Davila and L. D. Marks, *Acta Cryst.* **B53**, 916 (1997).
59. R. W. Gerchberg and W. O. Saxton, *Optik* **35**, 237 (1972).
60. J. R. Fienup, *Optics Lett.* **3**, 27 (1978).
61. J. R. Fienup, *J. Optical Soc. Am.* **4**, 118 (1987).
62. M. H. Hayes, *Image Recovery*: *Theory and Application*: *Reconstruction from Magnitude or Phase*, ed. H. Stark (Academic, Orlando, 1987), p. 209.
63. M. H. Hayes, *Image Recovery*: *Theory and Application*: *Reconstruction from Magnitude or Phase*, ed. H. Stark (Academic, Orlando, 1987), pp. 221–223.
64. D. L. Dorset, *Structural Electron Crystallography* (Plenum, New York, 1995), pp. 128–133.
65. M. M. Woolfson and H. Fan, *op. cit.*, pp. 34–65.
66. G. Jayaram, P. Xu and L. D. Marks, *Phys. Rev. Lett.* **71**, 3489 (1993).
67. A. E. H. Love, *A Treatise on the Mathematical Theory of Elasticity* (Dover, New York, 1944), p. 172.
68. F. Jona, J. A. Strozier Jr. and W. S. Yang, *Rep. Prog. Phys.* **45**, 527 (1982).
69. *International Tables for Crystallography*, ed. T. Hahn (Kluwer, Dordrecht, Netherlands, 1989), pp. 82–99.
70. T. Takahashi and S. Nakatani, *Surf. Sci.* **282**, 17 (1993).
71. M. Foss, R. Feidenhans'l, M. Nielsen, E. Findeisen, R. L. Johnson, T. Buslaps, I. Stensgaard and F. Besenbacher, *Phys. Rev.* **B50**, 8950 (1994).
72. M. Foss, R. Feidenhans'l, M. Nielsen, E. Findeisen, T. Buslaps, R. L. Johnson and F. Besenbacher, *Surf. Sci.* **388**, 5 (1997).
73. L. Lottermoser, T. Buslaps, R. L. Johnson, R. Feidenhans'l, M. Nielsen, D. Smilgies, E. Landemark and H. L. Meyerheim, *Surf. Sci.* **373**, 11 (1997).
74. A. H. Levermann, P. B. Howes, K. A. Ewards, H. T. Anyele, C. C. Mathai, J. E. Macdonald, R. Feidenhans'l, L. Lottermoser, L. Seehofer, G. Falkenberg and R. L. Johnson, *Appl. Surf. Sci.* **104**, 124 (1996).